

**ASSESSMENT OF SEABED MUNITION MOBILITY
INDUCED BY PROPELLER-GENERATED TURBULENCE**

by

Christopher Q. Swanson

A thesis submitted to the Faculty of the University of Delaware in partial fulfillment of the requirements for the degree of Master of Science in Ocean Engineering

Fall 2025

© 2025 Christopher Q. Swanson
All Rights Reserved

**ASSESSMENT OF SEABED MUNITION MOBILITY
INDUCED BY PROPELLER-GENERATED TURBULENCE**

by

Christopher Q. Swanson

Approved: _____
Jack A. Puleo, Ph.D.
Professor in charge of thesis on behalf of the Advisory Committee

Approved: _____
Rachel A. Davidson, Ph.D.
Chair of the Department of Civil, Construction, and Environmental Engineering

Approved: _____
Pamela M. Norris, Ph.D.
Dean of the College of Engineering

Approved: _____
Gary T. Henry, Ph.D.
Interim Vice Provost and Dean of the Graduate College

ACKNOWLEDGMENTS

I would like to express my deepest gratitude to my professor and thesis advisor, Dr. Jack Puleo, for all his helpful advice, guidance, and feedback over the past two years. Additionally, I am deeply indebted to Dr. Tyler Van Buren for his work assisting as co-supervisor on this project. This work was made possible through the invaluable support of SERDP, which generously financed this project. We also extend our sincere gratitude to the Lewes Campus and its resolute boat captain for providing essential site access, crucial boat support, and invaluable assistance in determining initial site locations. Additionally, I am grateful to Chinoye Agadi who has been a useful partner in this research. Special thanks to all the many members of the Center for Applied Coastal Research (CACR) and VanBuren Labs Mechanical Engineering students for their help in the construction and monitoring of the living shoreline, including Frank Tricouros, Sam Meyer, and Parker Grobe. Finally, I would be remiss in not thanking my fiancée LT Renée Hill who has supported me without reserve during my time away from the Navy. Your unending love and support have ensured the success of this part of our journey.

TABLE OF CONTENTS

LIST OF FIGURES	vi
LIST OF TABLES	viii
ABSTRACT.....	ix
Chapter	
1 INTRODUCTION	1
1.1 Background.....	1
1.2 Munitions Mobility, Burial, and Transport	3
1.3 Sediment Transport	5
1.4 Propeller Wash	6
1.5 Scaling.....	9
2 METHODS	18
2.1	18
2.2	27
2.3	29
3 RESULTS.....	31
4 DISCUSSION	35
4.1 Optimal Location For Maximum Displacement	35
4.2 Target Size and Density Difference	35
4.3 Average Velocities.....	36
4.4 Shields Parameter.....	36
4.5 Froude Number	37
4.6 Sliding Versus Rolling	38
4.7 Some Targets Initially Moved the “Wrong Way”	40
4.8 Lessons Learned.....	41
5 CONCLUSION.....	44
REFERENCES	46

LIST OF FIGURES

FIGURE 01. MAP OF KNOWN UXO IN THE CONTIGUOUS UNITED STATES OCEANS (REPRODUCED FROM ARCGIS)	2
FIGURE 02. US NAVY EOD INSPECTING UXO (REPRODUCED FROM RICK STABER, 2018)	2
FIGURE 03. HOW LOCAL MORPHODYNAMICS CAN EFFECT MUNITION STABILITY. MUNITION 1 HAS MUCH MORE LOCAL STABILITY THAN MUNITION 2	4
FIGURE 04. SCHEMATIC OF A PROPELLER JET (ADAPTED FROM HAMILL, 1987).	7
FIGURE 05. BOAT LENGTH VS PROPELLER DIAMETER.....	10
FIGURE 06. CURRENT METER TO CALIBRATE ELECTRIC OUTBOARD MOTOR SPEEDS VS INPUT AMPERAGE.....	12
FIGURE 07. ELECTRIC OUTBOARD MOTOR SPEEDS VS INPUT AMPERAGE ...	13
FIGURE 08. TARGET SCALING.	14
FIGURE 09. FINISHED TARGETS PRIOR TO USE IN THE EXPERIMENT. COLORS INDICATE SG (BLUE = 1.1, GREEN = 1.2, ORANGE (UNPICTURED) = 1.7, PINK = 2.2, RED = 3.2).	16
FIGURE 10. LARGE INDOOR POOL (NOTE THE TEST TARGETS THAT ARE MENTIONED LATER).	19
FIGURE 11. BOX OF SEDIMENT WITHIN LARGE POOL, EVALUATED MUNITIONS WERE PLACED INSIDE.	19

FIGURE 12. SEDIMENTS SIZE PERCENTAGES. NOTE THAT THE ORIGINAL SAND CAME WITH MANUFACTURERS TOLERANCES AND THAT SIEVE 250 IS THE PAN.....	21
FIGURE 13. THE SMALL POOL IS FILLED WITH MUDDY SEDIMENT. NOTE THE FINES “LEAKING” OUT OF THE SEDIMENT AS WATER IS ADDED WITHOUT ANY AGITATION.....	22
FIGURE 14. THE EXTRUDED ALUMINUM 80/20 MOTOR MOUNT. NOTE HOW THE MOUNT COULD BE LIFTED AND MOVED TO ANY LOCATION ALONG THE LENGTH OF THE POOL.....	23
FIGURE 15. THE BTR LIFEP04 BATTERIES (48, 60 AH).....	23
FIGURE 16. ASSESSING THE SONAR. THE RAW DATA FROM FIGURE 17 MATCHES UP TO THESE TARGETS.....	25
FIGURE 17. MATLAB 3D PLOT OF THE TEST TARGETS. NOTE HOW THE “SHADOWS” FROM THE OTHER ITEMS AND THE CIRCULAR SCANNING METHODS DISORIENTED THE SHAPE. FLATTER SURFACES SHOWN LATER DID NOT HAVE THESE “SHADOWS.”	26
FIGURE 18. 10 CM X 10CM GRID SYSTEM	27
FIGURE 19. TESTING SET UP, NOTE THE ANGLE AND DISPLACED SEDIMENT LOWERING THE POOL VISIBILITY.....	28
FIGURE 20. LOCATION OF LEWES TESTING AREA.	29
FIGURE 21. TARGET DISPLACEMENT FROM PROPELLER WASH	32
FIGURE 22. POTENTIAL NON-SYMMETRICAL FLOW OVER A CYLINDER	41

LIST OF TABLES

TABLE 01. PROPELLER CHARACTERISTICS THAT AFFECT MUNITIONS IN SEDIMENT MOTION	8
TABLE 02. TWIN SCREW BOAT LENGTH TO PROPELLER DIAMETER RATIO DATA.	11
TABLE 03. TARGET WEIGHTS AND BUOYANCY FORCES (THE BUOYANCY OF THE LARGER TARGETS ARE 2.12X THE SMALLER TARGETS)	16
TABLE 04. SIZE DISTRIBUTION OF DELIVERED SEDIMENT AS PER INDUSTRIAL SOURCE	20
TABLE 05. SONAR PARAMETERS	24
TABLE 06. TESTING MATRIX	27
TABLE 07. LEWES SEDIMENT SAMPLE.....	30
TABLE 08. DISPLACEMENT OF MUNITIONS BASED ON SPECIFIC GRAVITY AND DISTANCE FROM THE PROPELLER.....	31
TABLE 09. REYNOLDS NUMBER FOR EACH TARGET	34
TABLE 10. AVERAGE VELOCITIES FOR EACH TEST	36
TABLE 11. TARGETS ROLLING VS SLIDING	39
TABLE 12. TARGETS THAT MOVED INTO PROP WASH INITIALLY	40

ABSTRACT

In the years prior to the contemporary environmental movement, navies around the world dumped unused munitions overboard for disposal. In 1972, the London Convention banned many pollutants, including munitions. Half a century since, these potentially live munitions can come onshore or be uncovered by erosion, posing serious risks to the public. Among the mechanisms driving munitions mobility, this study investigates the influence of propeller generated turbulence on munitions transport. The experiment used a large pool with a sediment bed and a proud munition model (also referred to as target). An overhead outboard motor was used to simulate vessel propeller wash. Results showed munition density was a parameter governing target stability under propeller-generated flows. Targets constructed to emulate high density conventional munitions demonstrated strong resistance to displacement by not exhibiting movement under tested flow regimes. In contrast, movement was observed only when the targets were configured to be less than half as dense as conventional ordnance. Detailed measurements further established that the magnitude of target displacement was governed by density and sensitive to spatial proximity to the propeller; targets positioned near the point of maximum jet velocity experienced substantially larger mobilization. The patterns affirm that, in deep-water scenarios where propeller-induced turbulence dissipates rapidly and munitions remain dense, the overall risk of large-scale munition migration is low. Nevertheless, there is a heightened vulnerability for less dense munitions or scenarios characterized by high-energy, confined settings—such as navigation channels and high traffic port facilities—where persistence of strong, localized flows can present a mobilization threat. The ability to predict munition movement, combined with general historical disposal data are crucial to predict when/where expected munitions may arise. Local authorities can then exclude the populace until ordnance experts can properly dispose of them in a safe and formal process, akin to the Iron Harvest in northern France.

Chapter 1

INTRODUCTION

1.1 Background

Unexploded ordnance (UXO, also called munitions) were historically disposed of by dumping overboard before returning to port. In the United States (US), the practice of vessels dumping munitions mostly occurred during the World Wars and ended in 1969. Most other world navies stopped shortly after in 1975 with the signing of the London Convention on the Prevention of Marine Pollution by Dumping of Wastes, also for environmental reasons (Ong et al., 2010). In the US, all oceanic coasts are affected (Figure 01), with only the Great Lakes being spared. There are over 450 underwater sites across the US that may be contaminated with munitions (SERDP, 2018). Most UXO on the west coast are centered around the three major area approaches of Puget Sound, San Francisco Bay, and the Channel Islands. On the east coast, UXO are much more evenly spread (Figure 01). UXO can vary from chemical munitions that leak out into the environment or traditional high explosive rounds (Figure 02).



Figure 01. Map of known UXO in contiguous United States (Reproduced from ArcGIS).



Figure 02. US Navy EOD inspecting UXO (Reproduced from Rick Staber, 2018).

Ship captains attempted to dump in deep water far from land to cause the least amount of impact. The dynamic nature of the marine environment and ongoing human activities mean a small percentage leave their initial disposal locations. Tides, storm

surge, and wave action can all affect the scouring or burying of UXO and the natural slope of the seafloor can enhance or hinder movement (Colangeli et al., 2024, Whitehouse et al., 2011). Human processes include dredging (for either navigation or beach nourishment), anchoring, underwater infrastructure construction (e.g., cable lines, wind farms, offshore pipelines, bridges/tunnels) and vessel traffic propeller wash. UXO continue to pose a serious threat along US coastlines, where items have appeared onshore and required either safe disposal or detonation in place. With over 40% of the US population living in coastal counties (NOAA, 2021), the risk of human contact with UXO is notable. Due to navigational constraints, naval vessels often adhered to established shipping lanes when entering ports, inadvertently depositing munitions into high-traffic routes also used by civilian vessels (San Diego Bay, Norfolk, James/Elizabeth Rivers as well as entry to into the Chesapeake) (SERDP 2018). The constant maneuvering of ships as they enter and exit the port causes particle suspension and potentially the burial or transport of UXO.

1.2 Munitions Mobility, Burial, and Transport

Munitions mobility depends on the local forces. Hydrodynamic forcing of near bed flow velocities generated from hurricane level winds only cause minor horizontal displacement (Ganju et al., 2024). Hurricane high winds caused burial in 50% to 100% of the surrogate munitions depending on sediment composition and hydrodynamic energy.

The local bed morphodynamics will affect UXO mobility. For example, UXO may be more likely to transport downslope or remain in place if located between two local elevation maxima (Figure 03; Whitehouse et al., 2011). Also, the distance from the shore within the different zones (swash, surf and offshore) of the nearshore profile change the probability of transportation (Idowu et al., 2024). In the swash zone the UXO exhibit a slightly skewed probability of onshore or offshore migration. Onshore forcing can sometimes lead to munitions being trapped in bathymetric depressions seaward of the berm. In the surf zone, migration was slightly offshore directed in 65% of observations

(Idowu et al., 2024). The surf zone recorded the largest migration distances, primarily influenced by downslope gravity. Finally, for offshore migration is slightly onshore-dominant (65% of observations), often attributed to skewed waves over flat bathymetry. Differences in the zones include factors such as wave heights/periods, the depth, and importantly the local profile all affected the mobility or lack thereof (Cristaudo et al., 2023).



Figure 03. How local morphodynamics can effect munition stability. Munition 1 has much more local stability than Munition 2.

Munition mobilization in dynamic coastal environments is fundamentally governed by a moment balance if it will roll, where an object moves when destabilizing forces overcome stabilizing forces. Varying hydrodynamic conditions during uprush and backwash generate critical forces, including drag, lift, and fluid acceleration, that directly induce or resist motion. (Cristaudo et al., 2023). Object-specific properties such as density, shape, and initial burial depth significantly dictate mobility, with less dense and less-buried munitions exhibiting greater propensities for movement. Continuous interaction with the mobile sandy seabed, leading to scour and reburial, dictates short-term migration and the long-term fate of munitions within the active transport zone (Cristaudo et al., 2023).

1.3 Sediment Transport

Forces supplied to the bed may exceed the threshold of motion criterion for sediment. The criterion for the initiation of sediment motion is fundamentally governed by the balance between the bed shear stress exerted by the flow and the effective submerged weight of the sediment particles (Shields, 1936). The relationship is expressed through the Shields parameter; a dimensionless quantity defined as the ratio of the critical bed shear stress required to initiate motion to the gravitational force acting on the particle as

$$\theta = \frac{\tau}{(\rho_s - \rho)gd}, \quad (01)$$

where θ is the Shields Parameter, τ is the bed shear stress exerted by the fluid, ρ_s is sediment density, ρ is the fluid density, g is gravitational acceleration, and d is the particle diameter. By estimating the bed shear stress (and subsequently the Shields number for incipient motion) from the velocity that leaves the propeller and a friction coefficient, and applying a quadratic drag law, the bed forces can be estimated (Blaauw and van de Kaa, 1978). However, the method inadequately accounts for the complex turbulence or large-scale coherent structures.

A commonly used dimensionless number in hydrodynamics is the Reynolds number (Re). Re is the ratio between inertial and viscous forces, commonly used to differentiate between laminar and turbulent flow,

$$Re = \frac{\rho vL}{\mu}. \quad (02)$$

In this case, the velocity scale (v) is speed that the water passes around the target munition, L is the length of the munition parallel to the water flow direction and μ is the dynamic viscosity of the water.

The Froude number (Fr) is a fundamental dimensionless parameter in fluid mechanics that quantifies the ratio of inertial forces to gravitational forces that are acting

within a fluid flow, particularly relevant in open channel hydraulics and free-surface flows

$$Fr = \frac{v}{\sqrt{gL}}, \quad (03)$$

where v again is a characteristic velocity, and L a characteristic length scale such as flow depth. The Froude number serves as a critical indicator of flow regimes: subcritical ($Fr < 1$), critical ($Fr = 1$), and supercritical ($Fr > 1$). Subcritical flows are dominated by gravitational forces and tend to be tranquil with waves able to propagate upstream, while supercritical flows are inertia-dominated with rapid, often turbulent behavior where disturbances are only carried downstream. Fr use enables similarity modeling across different scales by maintaining dynamic equivalence of gravitational and inertial effects, making it useful for predicting flow behavior.

1.4 Propeller Wash

Vessels generate locomotion via oars, wind, propellers, or water jet action, with the most common method today being propellers or prop for short. Hydrodynamic forces from the thrust spread outward and downward injecting turbulence and large-scale coherent structures that may interact with the sea bed (Yuksel et al., 2017). The moving volume of water is turbulent and has these typical characteristics (Figure 04). The phenomena is commonly called “prop wash”.

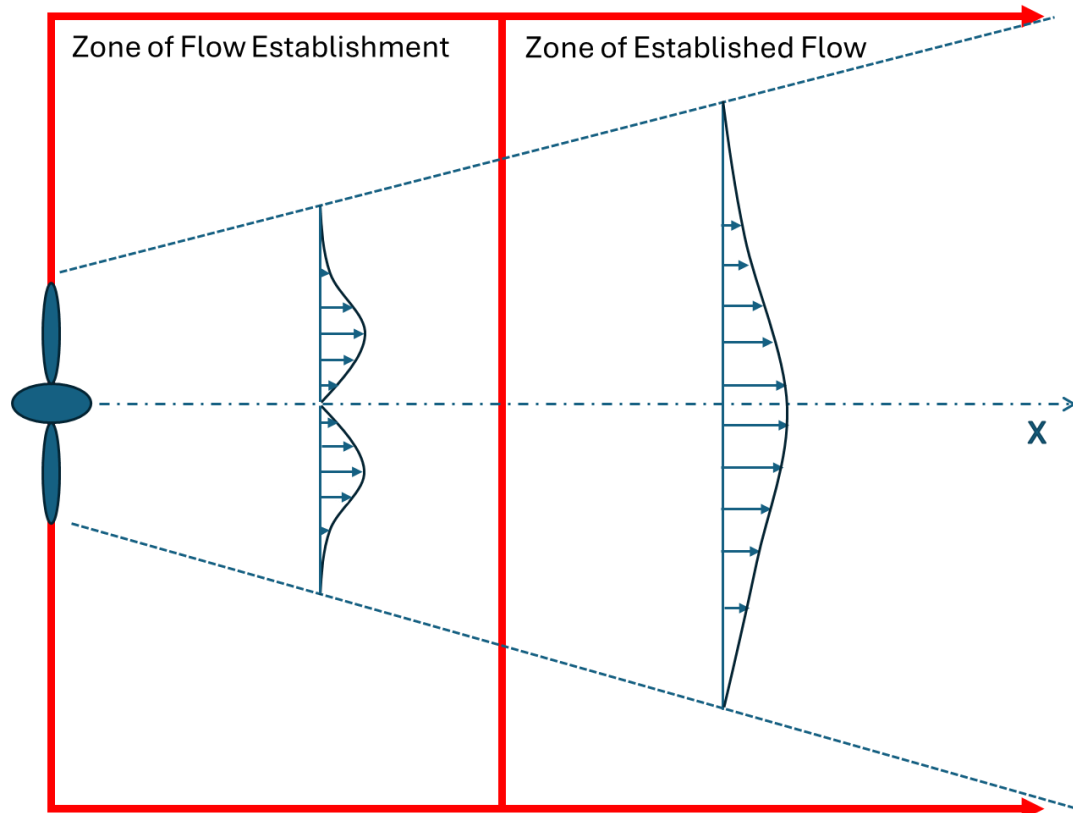


Figure 04. Schematic of a propeller jet (adapted from Hamill, 1987).

Prop wash generates complex hydrodynamic forces characterized by extreme turbulence with distinct three-dimensional velocity components. The propeller directly controls the magnitude from the thrust, torque, and the vessel advance velocity (Hashim, 1993). The propeller characteristics that affect the sediment are summarized in Table 01. An object within or resting on the seabed can induce a scour hole when subjected to hydrodynamic forces. Scour holes are caused by localized high pressure zones that push sediment away. (Oldenhof, 2021). The velocity distribution behind the propeller can be conceptualized in two distinct regions: a flow establishment zone and an established flow zone (Figure 04; Hamill, 1987). In the flow establishment region, the mean velocity profile typically exhibits two symmetrical peaks about the x axis, which subsequently merge into a single, less pronounced maximum within the established flow region. The

velocity gradients and inherent rotational motion within the flow will shed turbulence that will spread laterally and downward (Tan et al., 2017).

Table 01. Propeller characteristics that affect munitions in sediment motion.

Munition characteristics	Size	Orientation	Weight / Density distribution	Current level of burial (fully submerged, partial % or proud)
Sediment characteristics	Density	Size distribution	Material	
Propeller characteristics	RPM	Diameter	Vertical Angle (i.e., negative trim)	Number of Blades
Vessel Characteristics	Engine Power	Vessel Speed	Impeller vs. Propeller	Depth from Propeller to Sediment

UXO can be moved by prop wash by multiple methods. First, and the least likely, is that the generated turbulence is enough to physically mobilize a proud UXO. The second way UXO can be mobilized is if the sediment around them moves and the UXO shifts. For the first option to happen, the UXO forces would have to be minimized while the acceleration is maximized. For example, to minimize drag forces the UXO would have to be unburied, have minimal density and roughness. Buried munitions have minimal surface area for hydrodynamic forces to act on, plus the addition of a suction force (Cristaudo et al., 2023). 20th century munitions are dense and have tended to bury themselves hence their limited mobility over the past 50 years. On the other side of the force balance, acceleration forces would come from powerful engines close to the seafloor. Shallow water port entries force propellers closer to the seafloor, which generates stronger turbulent flow that reaches the bottom; however, most shallow sections of navigational channels enforce strict no-wake restrictions of five knots limiting prop wash. The second method can happen when sediment is displaced in such a manner that the UXO placement is no longer stable, leading to its displacement (Figlus et al., 2024). The instability could potentially come from a scour hole and undermine the UXO by reducing the bearing capacity although this could cause munition burial as well.

Flow that displaces sediment and destabilizes UXO placement can cause shifting. (Baranwal et al., 2024). Depending on munition orientation and the seafloor slope, forces can alter the sediment, allowing the UXO to begin rolling or sliding down the slope. Downhill sliding could indicate a movement out to sea. (Foster et al., 2020).

Turbulence produces a pressure difference from the flow via Bernoulli's principle, and the difference generates a lift force (Zanke, 2003). The lift force generated by modern boat operations is orders of magnitude too weak to move conventional 20th century munitions. (Landa et al., 2020). While the lift force might not physically lift the munition, it could reduce the forces on the munition, making it easier to displace. However, these lifting forces and tangential stresses could potentially lift the surrounding sediment. A stationary UXO can become unburied when forces displace the surrounding sediment, allowing natural coastal processes to potentially move it more freely.

A laboratory study will be undertaken to investigate the effect of prop wash on munitions that are proud on a sediment bed. The munitions will have various densities and be located at different distances from the propeller. Testing will assume a single pass of a US Navy Destroyer steered over the munition. Data will be used to demonstrate potential for UXO mobility, including if inert munitions have been mobilized. The results will directly benefit the Navy and the DoW through knowledge of the forces that prop wash delivers to the seabed during berthing operations; the potential to exhume and/or transport munitions, and possible strategies to avoid undesired munitions transport.

1.5 Scaling

Proper testing should be completed at scale because the forces acting on the sediment bed do not scale easily. For example, reducing the target size to match a reduced smaller engine size, would yield an incorrect ratio of prototype to scaled hydrodynamic forcing and affect the drag and lift forces on the target. However, reducing the size of the sediment is not plausible as the grains would then enter the cohesive regime.

Still, the project at this stage requires a scaling attempt due to unavailability of full-scale options. The Mobility Number (M) was chosen as the scaling variable as it relies on munition diameter (D), fluid velocity (u), and density via specific gravity (SG).

$$M = \frac{u^2}{(SG-1)gD} \quad (04)$$

The diameter and density of the actual UXO are known. Expected ship characteristics are needed (Figure 05) to model the fluid velocity. Once determined, multiple targets of varying diameters and densities can be designed for scaled testing. Vessel length for various designs grows by approximately 33 m for every meter increase in propeller diameter (Table 02).

The propeller in this study has a diameter of 0.15 m (6”) and represents a vessel with a length of approximately five meters (16’ 4”). A five-meter vessel would be approximately a small inland boat carrying ~3 people and gear for a fishing trip for visualization purposes.

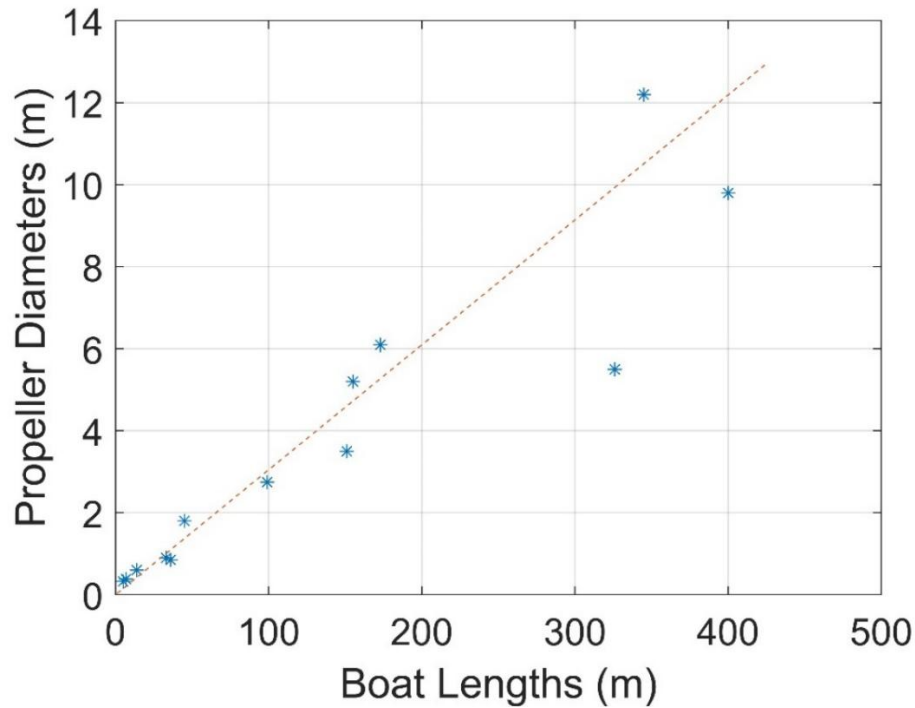


Figure 05. Boat Length vs Propeller Diameter.

Table 02. Twin screw boat length to propeller diameter ratio data.

Boat Type	Boat Length (m)	Propeller Diameter (m)	Specific Boat Used	Notes
Recreational Boat	5	0.33	General	Built for recreation
RHIB	7	0.38	General	Navy
R/V Daiber	14	0.6	R/V Daiber	Research Vessel
Yard Patrol	33	0.9	YP 703 Class	Navy
R/V Sharp	36	0.85	R/V Sharp	Research Vessel
Yacht	45	1.8	General	Built for recreation
Corvette	99	2.75	Khareef Class	Navy (Oman)
Frigate	151	3.5	Constellation Class	Navy
DDG	155	5.2	Arleigh Burke Class	Navy
Cruiser	173	6.1	Ticonderoga Class	Navy
Cruise Ship	326	5.5	Norwegian Escape	Built for recreation
LNG Tanker	345	12.2	Q-Max Clas	Industrial
Shipping Container Ship	400	9.8	Maersk Triple E Class	Industrial

Calibration to determine the optimal propeller speed employed a JFE Infinity EM Current Meter. The JFE was mounted 0.5 m from the propeller and 0.45 m (hub height) above the sediment bed (Figure 06). The distance of 0.45 m was the closest the electric outboard could be safely lowered in the water column. The distance of 0.5 m away from the propeller is where the flow converged from two lobes into established flow (Figure 06).

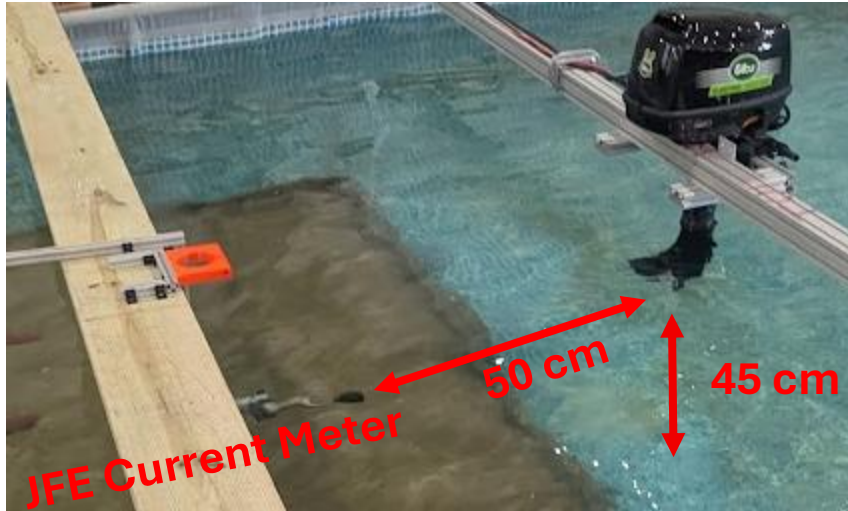


Figure 06. Current Meter to calibrate electric outboard motor speeds vs input amperage.

Tests were conducted with the electric outboard motor at every 5 Amps from 5 to 50 A with each one being tested for 1 minute. (Figure 07). After each test, the water was rested for five minutes to minimize the effects of circulation in the pool. The electric outboard was moving water in the tenths of meters per second order of magnitude. Battery limitations capped the amperage for sustained testing. To simulate as close to a step function of prop wash that the seafloor feels when a boat passes over it, 35 A was chosen as the final testing power for the motor so a shorter ramp up time to speed would be evaluated with. A value of 35 A correlates with a speed of 0.15 m/s (felt at hub height of 0.45 m above the bed).

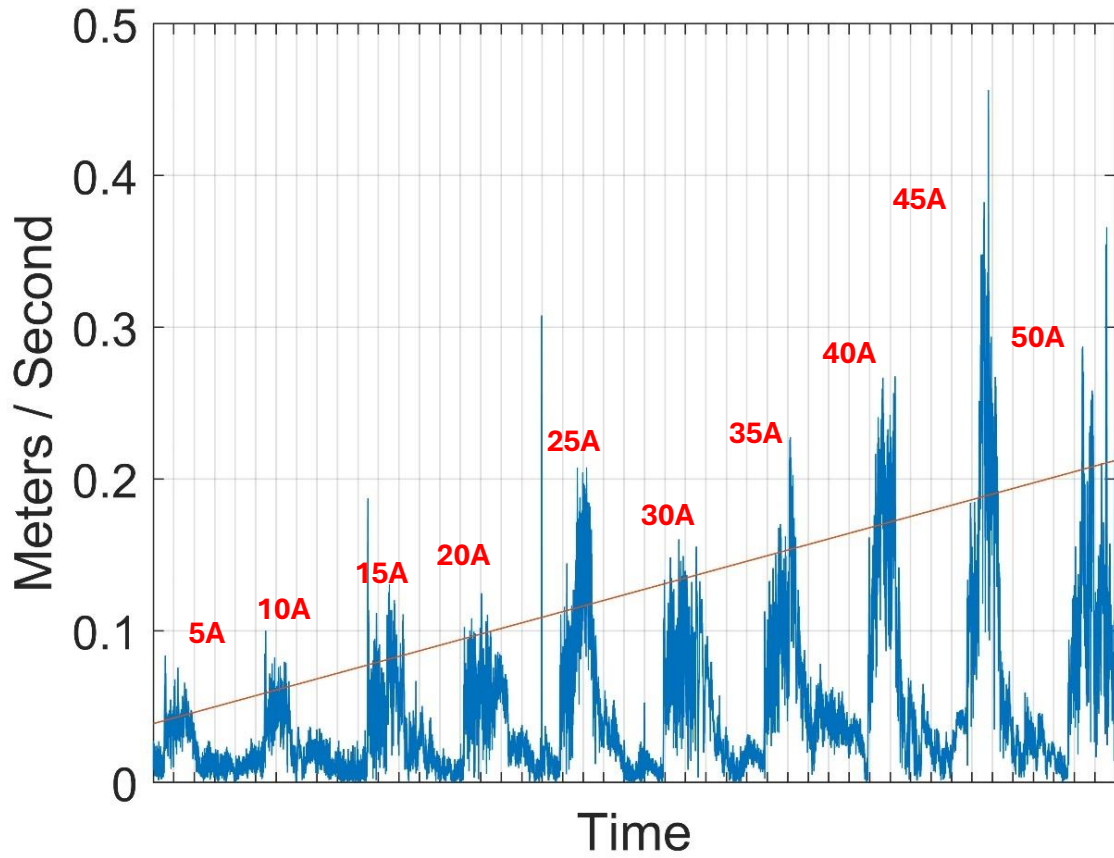


Figure 07. Electric outboard motor speeds vs input amperage.

The propeller was scaled down and unable to move full size targets. Thus, targets were also scaled for the study. Re and M scaling suggests the ratio of munition diameter should be

$$D_{Model\ Muntion} = D_{Muntion} \frac{SG_{Muntion}^{\frac{1}{3}}}{SG_{Model\ Muntion}^{\frac{1}{3}}} \quad (05)$$

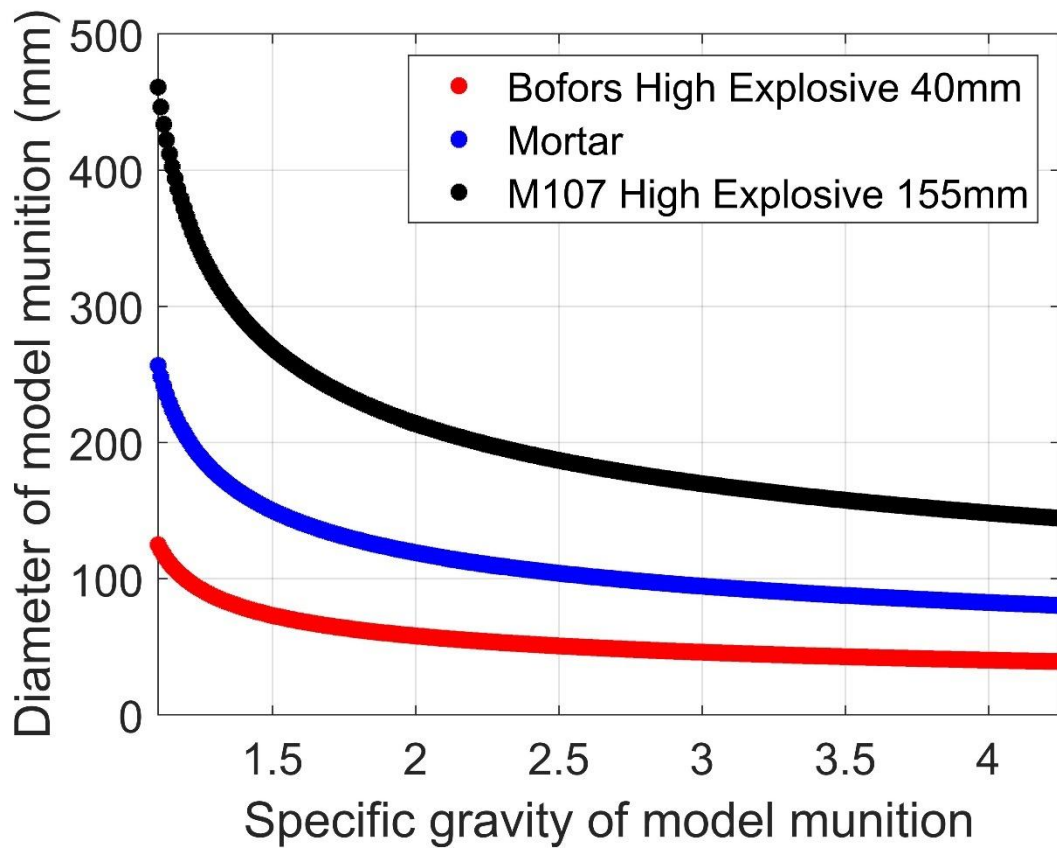


Figure 08. Target Scaling.

Most real-world conventional munitions that were dropped into the ocean have an SG in the range of 3.5 to 4.5. The scaling methodology dictates a target length of ~100 mm to achieve the desired mimicry of an 81mm mortar by the prototype. In the making of custom targets, the easiest and fastest way decided upon was to use a pipe that was filled with foam, sand, metal and water to obtain the proper uniform weight which was calculated based on the required density. The value of 100 mm is 3.94 inches so a four-inch pipe with an outer diameter of 4.5 inch (114.3 mm) was chosen for convenience. A 3.5-inch outer diameter (88.9 mm) was also chosen for a secondary diameter to evaluate. The experiment required setting the mobility number of the model munition equal to the mobility number of the UXO to determine the appropriate densities. The range of SG

values was set to be between 1.1 and 4.2. However, as shown in Section 4, the 2.2 and 3.2 SG targets did not move, so the planned 4.2 SG target was not constructed. Instead, an additional target with an SG of 1.7 was fabricated instead as the > 2.0 SG was the most critical density zone. *M* scaling shows that the less dense an object is, the more likely it is to move.

The targets were color coded to match the previous laboratory color scale (Figure 09; Table 03). Each of the ten targets was constructed with PVC pipes and filled with a mixture of foam, sand, metal and water depending on the target density. All targets were designed to be filled completely with water before the ends were duct taped, and final weight confirmed. The duct tape led to ease of construction and/or reconstruction as needed. As duct tape would not be waterproof and water would leak in, the targets were designed to be at proper weight when already waterlogged so that their density/weight would be correct when submerged and tested upon.



Figure 09. Finished targets prior to use in the experiment. Colors indicate SG (Blue = 1.1, Green = 1.2, Orange (unpictured) = 1.7, Pink = 2.2, Red = 3.2).

Table 03. Target weights and buoyancy forces (The buoyancy of the larger targets are 2.12x the smaller targets).

SG	Weight (kg) for 8.9 x 52.8 cm	Weight (kg) for 11.4 x 67.9 cm	Buoyancy Forces (N)
1.1 Blue	3.61	7.66	35.4 and 75.2
1.2 Green	3.93	8.36	38.6 and 82.0
1.7 Orange	7.21	15.33	54.7 and 116.2
2.2 Pink	10.49	22.29	70.7 and 150.3
3.2 Red	13.77	29.26	102.9 and 218.7

The mobility number calculations were based solely on a broadside thrust scenario. Using M to scale restricted the analysis to a single orientation, which effectively simulates a vessel passing directly perpendicular to the long axis of the model munition target. Consequently, the analysis focused exclusively on the maximum lateral force that could be applied to the munition by a passing vessel's propeller wash, representing the most susceptible condition for mobility.

This study did not examine the effects of munition lengths and eddy currents and hydrodynamic forces shedding from the ends of the target. The length was calculated by keeping the same length to diameter ratio as an actual 81mm mortar.

The electric outboard was run for five seconds to simulate a single pass of a vessel overhead. There was a two-second ramp up and ramp down on either end of this main five seconds to simulate the less powerful outer edges of the prop wash field. At a no-wake speed of five knots, a vessel moves 23 m (75') in this amount of time. Testing with this ramp up and ramp down will simulate the entire prop wash field passing over a munition,

The final scaling simulation will scale an Arleigh Burke Class US Navy Destroyer, traveling at a no-wake speed of five knots in a navigational channel making a single pass over an 81mm mortar round sitting proud on the sediment two meter below the propeller (14 m below the surface).

Chapter 2

METHODS

2.1 Laboratory Testing Set Up

Laboratory testing was conducted at the Center for Applied Coastal Research (CACR) at the University of Delaware. The experimental setup consisted of a sediment bed within a designated test basin, where various munition targets were positioned on the surface. Hydrodynamic forcing was generated by operating an outboard motor above the water surface, and the resulting changes in the munition surrogate positions were quantitatively assessed using a grid system of measurement. Originally, a rotary scan sonar was going to be used. The grid system was implemented when the sonar was not as useful as expected,. Key experimental parameters, including target diameter, the engine horizontal distance and munition density, were systematically varied. Between each experimental run, the sediment bed was reset to ensure consistency in initial conditions. Post-test analysis involved a comparison of results across all experimental conditions to determine the effects of the varied parameters on munition mobility.

The laboratory test had the following set up. A large, temporary above ground pool with dimensions of 5.5 m x 11 m (18' x 36') was filled to a depth of 1.1 m (3'7") (Figure 10). Inside the large pool, a wooden frame with a base of 3.05 m x 3.05 m (10' x 10') was filled with a sediment depth of 15 cm (6").

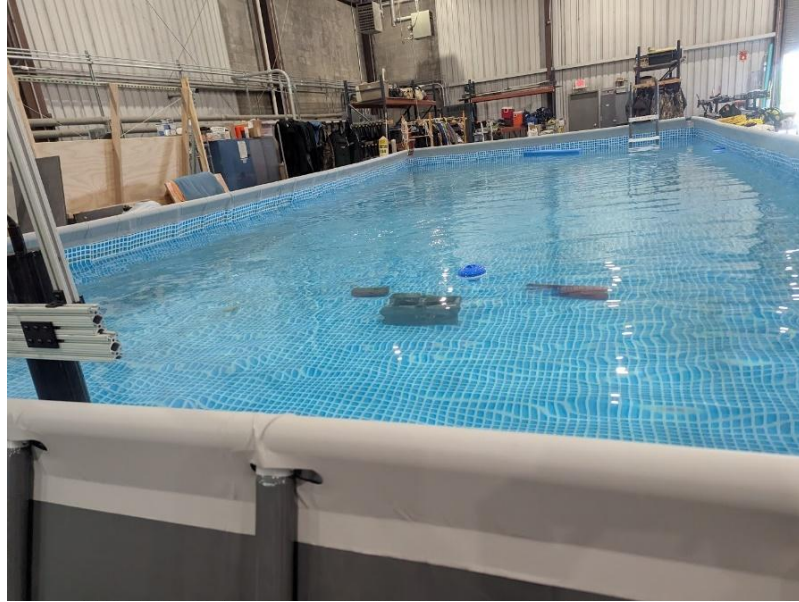


Figure 10. Large indoor pool (Note the test targets that are mentioned later). Image shows some initial testing without the sediment bed installed.

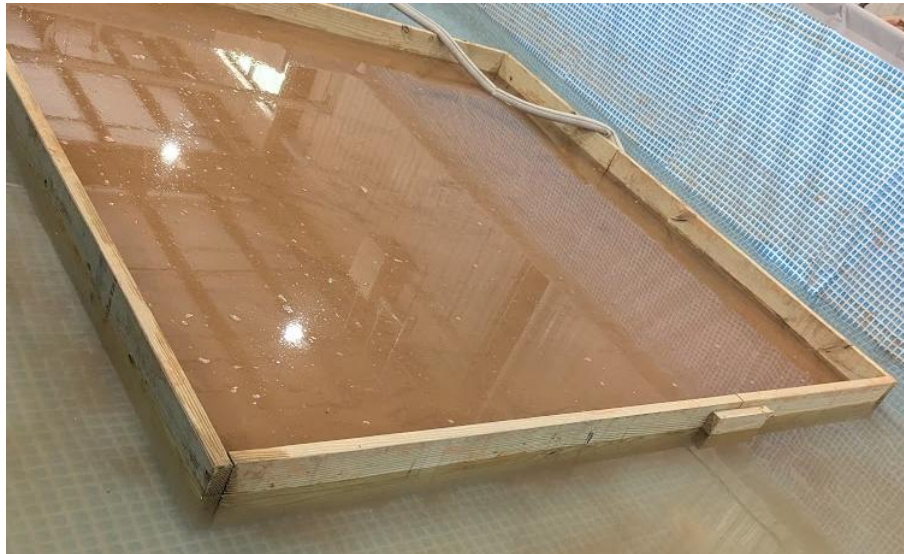


Figure 11. Box of sediment within large pool. Evaluated targets were placed inside.

The box was filled with sediment (#100; Construction Building Materials in Bensalem PA). Screen specifications expressed in mean percent retained in each sieve are shown in Table 04.

Table 04. Size distribution of delivered sediment as per industrial source.

ASTM E-11 Sieve #	Mesh Openings (mm)	#100 sediment Percentages
30	.600	0-10
40	.425	25-45
50	.300	20-40
70	.212	10-25
100	.150	10-25
140	.106	0-10
200	.075	0-5
PAN	-	0-5

The sediment specific gravity varied from 2.54 to 2.71. When mixed with water, all the fines became suspended and reduced visibility to less than one cm. The sediment was “cleaned” so that human eyes and underwater video cameras could see before, during, and after every test. Fines removal was achieved by placing the sediment in a smaller pool (Figure 12) sized 1.8 m x 3.6 m (6’ x 12’). Then the smaller pool was filled with water and the sediment agitated with a drill-mounted paddle paint mixer which was run in reverse to suspended fine grain sediment. While the fine grains of sediment were still suspended, the water and fine sediment mixture was pumped out, leaving only the larger grains (Figure 12).



Figure 12. The small pool is filled with muddy sediment. Note the fines “leaking” out of the sediment as water is added without any agitation.

The process took four “cleanings” before the sediment settled fast enough to enable visual inspection with a visibility of ~ 0.75 m within two minutes of no motion. Then, the sediment was shoveled from the small pool, into the box inside the large pool. The large pool was then filled with water.

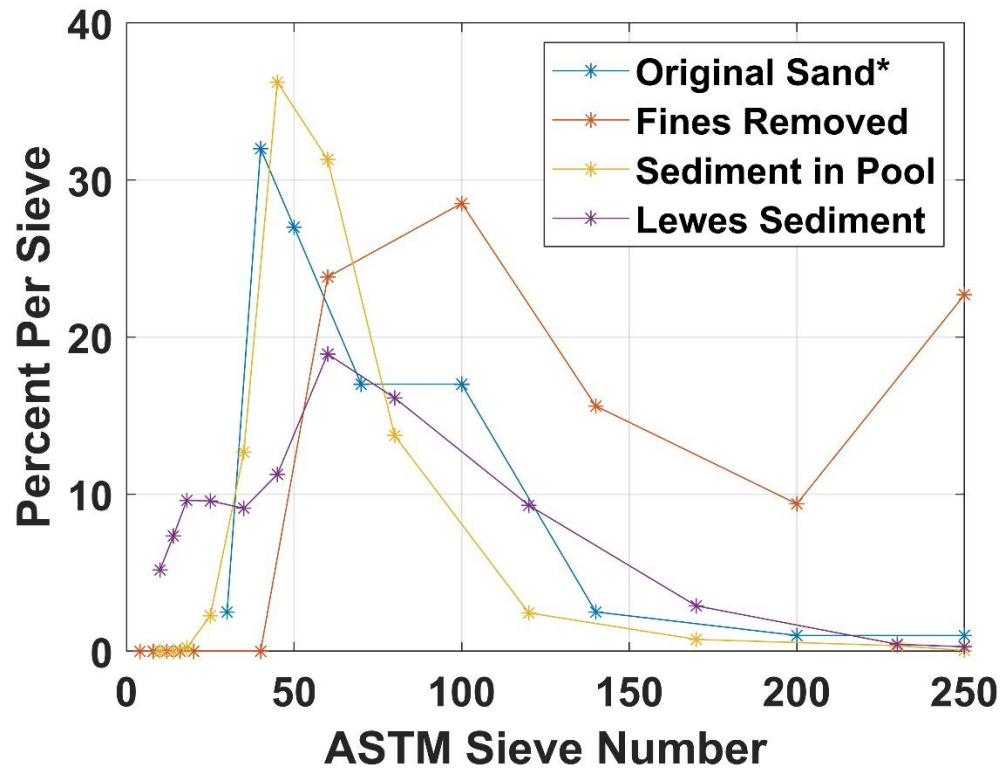


Figure 13. Sediments size percentages. Note that the Original Sand came with manufacturers tolerances and that Sieve 250 is the pan.

Outside of the pool, an electric outboard motor was mounted to a stand (Figure 14). The motor stand was created using 3.8 cm x 3.8 cm (1.5" x 1.5") extruded aluminum commonly known as "80/20". The motor was an Elco Model EP9.9RS rated for 7KW with a top mount throttle to control RPMs. The batteries (BtrPower) were LiFeP04 with 48V and a capacity of 60 Ah (Figure 15).

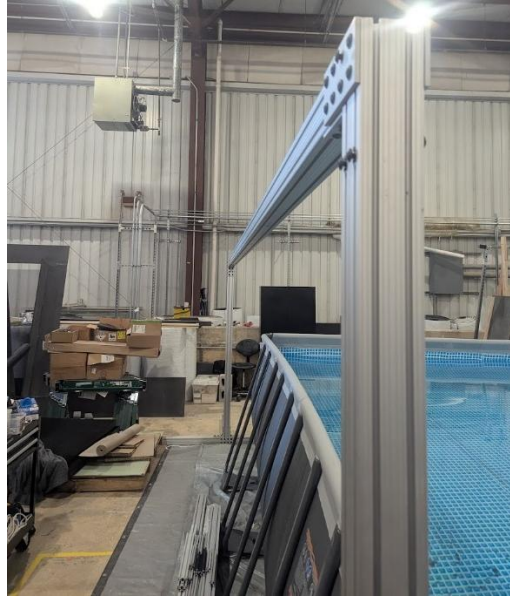


Figure 14. The extruded aluminum 80/20 Motor Mount. Note how the mount could be lifted and moved to any location along the length of the pool.



Figure 15. The BTR LiFeP04 Batteries (48, 60 Ah).

Table 05. Sonar Parameters.

Frequency	Tunable from 280 kHz to 1.1 MHz in 5 kHz steps
Transducer	Imaging type, fluid compensated
Transducer Beam Width	310 kHz: 4° x 40° 675 kHz: 1.8° x 20° 1 MHz: 0.9° x 10°
Range Resolution	1 m – 4 m: 2 mm (0.08”) 5 m & up: 10 mm (0.4”)
Range Scales (meters)	1, 2, 3, 4, 5, 10, 20, 30, 40, 50, 60, 80, 100, 150, and 200
Minimum Detecting Range	150 mm (6”)
Azimuth Angle	0 – 359.9 by 0.1° increments
Train Angles (Azimuth)	Continuous rotation, 0.1° increments
Elevation Angle	0 – 359.9 by 0.3° increments
Train Angles (Elevation)	Continuous rotation, 3° increments
Dimensions	669mm (26.34”) in height 303.5mm (11.95”) in length
Weight	Air: 9.5 kg (21 lbs.) Water: 3.3 kg (7.3 lbs.)
Materials	6061-T6 Aluminum & Polyurethane with anodization
Power Supply	20 – 36 VDC at less than 5 Watts

The sonar was calibrated by running tests with known target objects in the pool of known dimensions placed in certain orientations. The known objects included cinder blocks, regular bricks, and the test munitions (Figures 16 and 17). The sonar mounting had multiple iterations, but the best and final mounting was directly over the targets on a wooden board that spanned the whole pool (Figure 19). The output from the sonar was an .xyz file which had a row for each data point that consisted of that points spherical and

cartesian coordinates as well as the time that point was taken. The data were uploaded into MATLAB for plotting and visualization purposes.

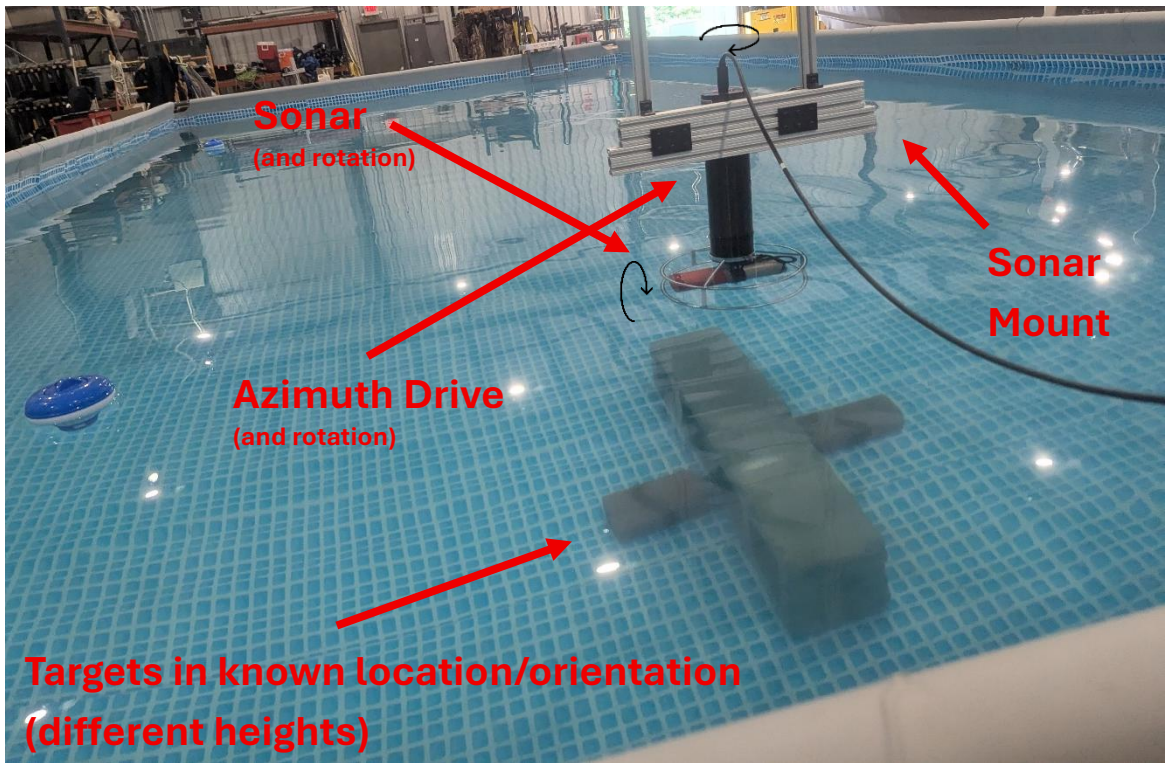


Figure 16. Assessing the Sonar. The raw data from Figure 17 matches up to these targets.

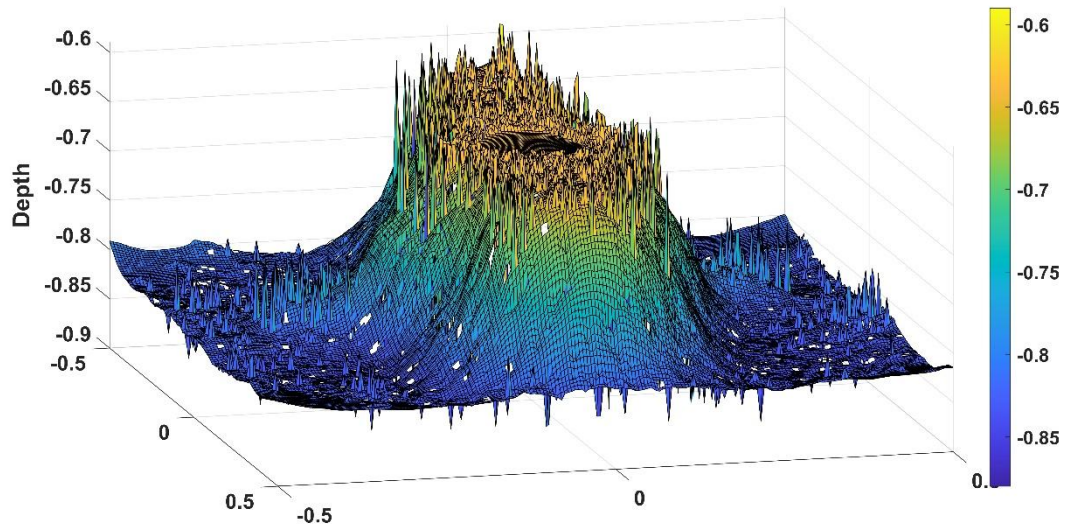


Figure 17. MATLAB 3D Plot of the test targets. Note how the “shadows” from the other items and the circular scanning methods disoriented the shape.

The sonar specs represented a much finer resolution than was attainable despite many months trouble shooting different methods to post process and discussing with the company. Thus, the sonar was eventually abandoned for use of measuring with a grid. The grid system was set up with metal hooks driven into the wooden sediment box edges at a fixed distance of 10 cm from each other (Figure 18). The (0,0) coordinate was the corner in Figure 19 shows “68 cm”. The measurement protocol defined the coordinates of all four target corners by counting the x- and y- distances from the (0,0) origin along the grid lines before and after running the motor. The grid method allowed for consistent and repeatable measurement of the target displacement within the sediment box to within 0.25 cm accuracy.



Figure 18. 10 cm x 10cm Grid System used for positioning targets.

2.2 Data Collection

A total of 40 different tests were identified via a Testing Matrix (Table 06). The various inputs that were settled upon was a set of 10 individual targets (two of each diameter for the five distinct specific gravities) that were to be tested at four different distances from the propeller.

Table 06. Testing matrix

Distance to Propeller	168 cm	208 cm	248 cm	288 cm
1.1 SG	9 x 53 cm Target	9 x 53 cm Target	9 x 53 cm Target	9 x 53 cm Target
	11 x 64 cm Target	11 x 64 cm Target	11 x 64 cm Target	11 x 64 cm Target
1.2 SG	9 x 53 cm Target	9 x 53 cm Target	9 x 53 cm Target	9 x 53 cm Target
	11 x 64 cm Target	11 x 64 cm Target	11 x 64 cm Target	11 x 64 cm Target
1.7 SG	9 x 53 cm Target	9 x 53 cm Target	9 x 53 cm Target	9 x 53 cm Target
	11 x 64 cm Target	11 x 64 cm Target	11 x 64 cm Target	11 x 64 cm Target
2.2 SG	9 x 53 cm Target	9 x 53 cm Target	9 x 53 cm Target	9 x 53 cm Target
	11 x 64 cm Target	11 x 64 cm Target	11 x 64 cm Target	11 x 64 cm Target
3.2 SG	9 x 53 cm Target	9 x 53 cm Target	9 x 53 cm Target	9 x 53 cm Target
	11 x 64 cm Target	11 x 64 cm Target	11 x 64 cm Target	11 x 64 cm Target

Also, two extra tests were run. The first was on targets already existing in the laboratory that are modeled after M151070 Hydra Rockets but with SG of 3.5 and 3.0. The second was once all calculations were done; the motor was run for a full minute to see an unimpeded large bed deformation.

During each test, an underwater camera was placed in opposite corners to capture the movement of the targets while being forced by the prop wash. The cameras were less useful than originally anticipated because targets often were not visible after initiation of motion within a suspended sediment cloud.. Although the footage was used to estimate the amount of displaced sediment.

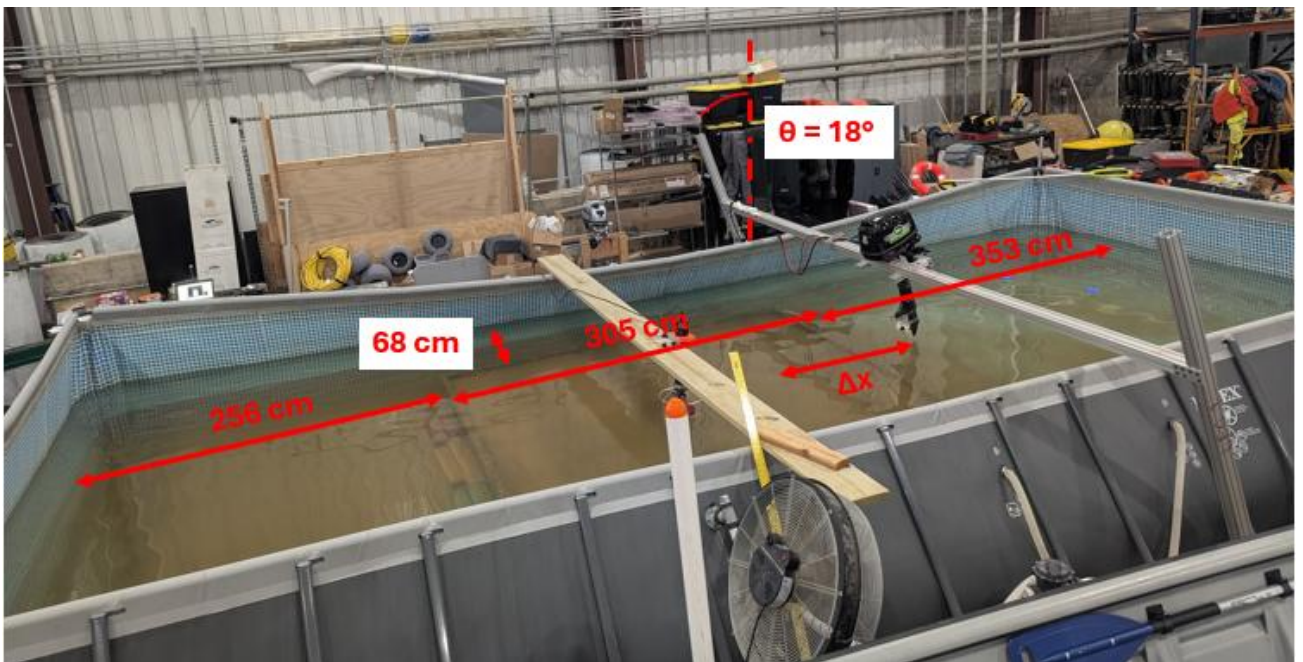


Figure 19. Testing set up, note the angle and displaced sediment lowering the pool visibility.

The speed of 0.15 m/s was well below the initial estimate of 1 m/s for mobility. So, the motor was tilted down by 18° (Figure 19) providing additional forcing for target migration. Also, compare this picture taken after the completion of testing to Figure 16 taken prior to testing and notice the sediment displacement and color of the water.

2.3 Lewes Preliminary Field Work

Field testing at Lewes was limited in scope due to logistical constraints, with two days of data collection completed on site.

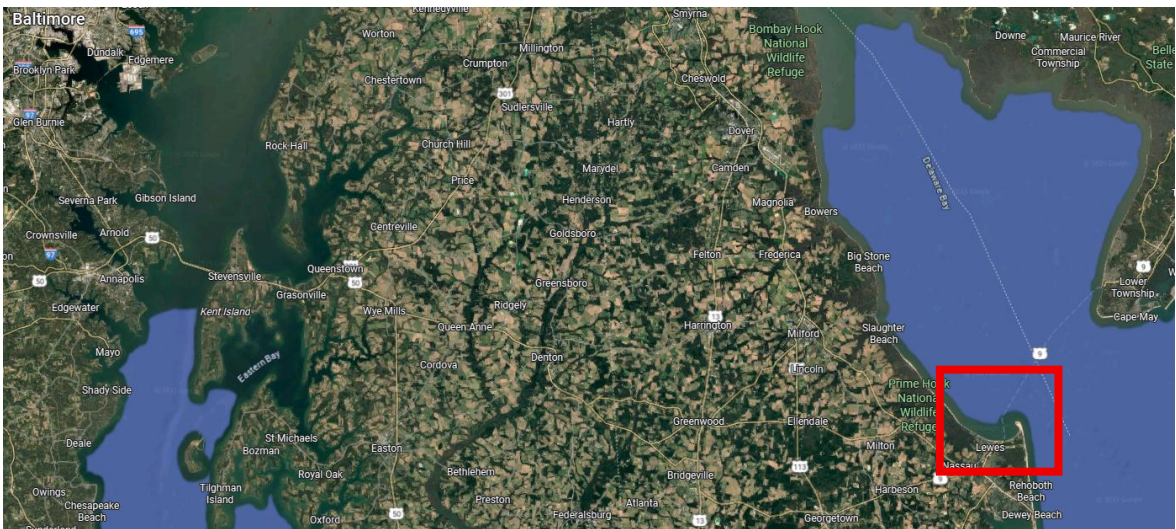


Figure 20. Location of Lewes testing area.

On the first day, four model munitions modeling the shape of an 81mm mortar and a M151070 Hydra Rockets were placed. They were placed and measured with GPS, then the R/V Daiber's twin 355 hp engines were run over them twice for 10 minutes at 900 RPM. Before the engines were run, then after both engine tests, a sonar scan was taken. However, this testing was completed when the sonar was thought to be gathering useful data. For time purposes, a less fine measurement was taken, but it still required an hour for each scan. The most visible feature that could be seen with the sonar scan was

that the bed sloped up the shore. The sound waves did not ping off the metal targets brightly compared to the mud they were placed in. At the end, divers retrieved the targets. All four targets were unburied and three remained in the exact same place and orientation in which they were placed. The least dense target, a 2.5 SG model of an 81mm mortar, moved ~4 m, in the same orientation, in line with the prop wash. A sample of the sediment that the targets were placed during field trials (Table 07; Figure 13).

Table 07. Lewes sediment sample

ASTM Sieve Number	Sieve Diameter (mm)	Weight Per Sieve (g)	% per sieve
10	2	1.65	5.2
14	1.4	2.34	7.3
18	1	3.06	9.6
25	0.71	3.05	9.6
35	0.5	2.9	9.1
45	0.355	3.59	11.3
60	0.25	6.03	18.9
80	0.18	5.14	16.1
120	0.125	2.96	9.3
170	0.09	0.92	2.9
230	0.063	0.14	0.4
Pan	-	0.09	0.3

The second day of testing was with a new method of positioning the sonar right above the targets, but without any improvement of high resolution scanning and the extreme length of time it took to get scans along with the logistics of transiting between the two sites prevented any more field testing for this phase of the study.

Chapter 3 RESULTS

Laboratory results were compiled by running the propeller at different distances from the targets and with different target densities (Table 08 and Figure 23). As expected, mobility of the targets increased with a decreasing distance between propeller and target as well as decreasing density.

Table 08. Displacement of munitions based on specific gravity and distance from the propeller.

	Distance to Propeller (cm)	168	208	248	288
1.1 SG	9 x 53 cm Target	67.28	122.72	81.79*	32.84*
	11 x 64 cm Target	73.99	111.85	80.96*	40.93*
1.2 SG	9 x 53 cm Target	96.39	137.07	68.31	0.00
	11 x 64 cm Target	68.85	117.21	32.73	0.00
1.7 SG	9 x 53 cm Target	70.25	20.35	0.00	0.00
	11 x 64 cm Target	106.02	0.25	0.00	0.00
2.2 SG	9 x 53 cm Target	0.00	0.00	0.00	0.00
	11 x 64 cm Target	0.00	0.00	0.00	0.00
3.2 SG	9 x 53 cm Target	0.00	0.00	0.00	0.00
	11 x 64 cm Target	0.00	0.00	0.00	0.00

* Stopped at the back wall

These data has four slightly skewed points. For the farthest tests away from the propeller for the blue targets with an SG of 1.1, they were prematurely stopped. They backed into the back wall of the sediment box. They likely would not have travelled much farther for two reasons. First, they were far from the main forceful center of prop wash. Second, being the least dense targets, they would have had a small amount of inertia. Although the underwater video contains significant suspended sediment that obscures visibility, the 11 x 64 cm target at the farther distance exhibited a rough top speed of approximately 0.25 m/s. Assuming the target is traveling half of that speed when it hits the wall (0.12 m/s), then it would still only have the momentum of \sim one kg m/s that would be quickly dissipated by the water and sediment.

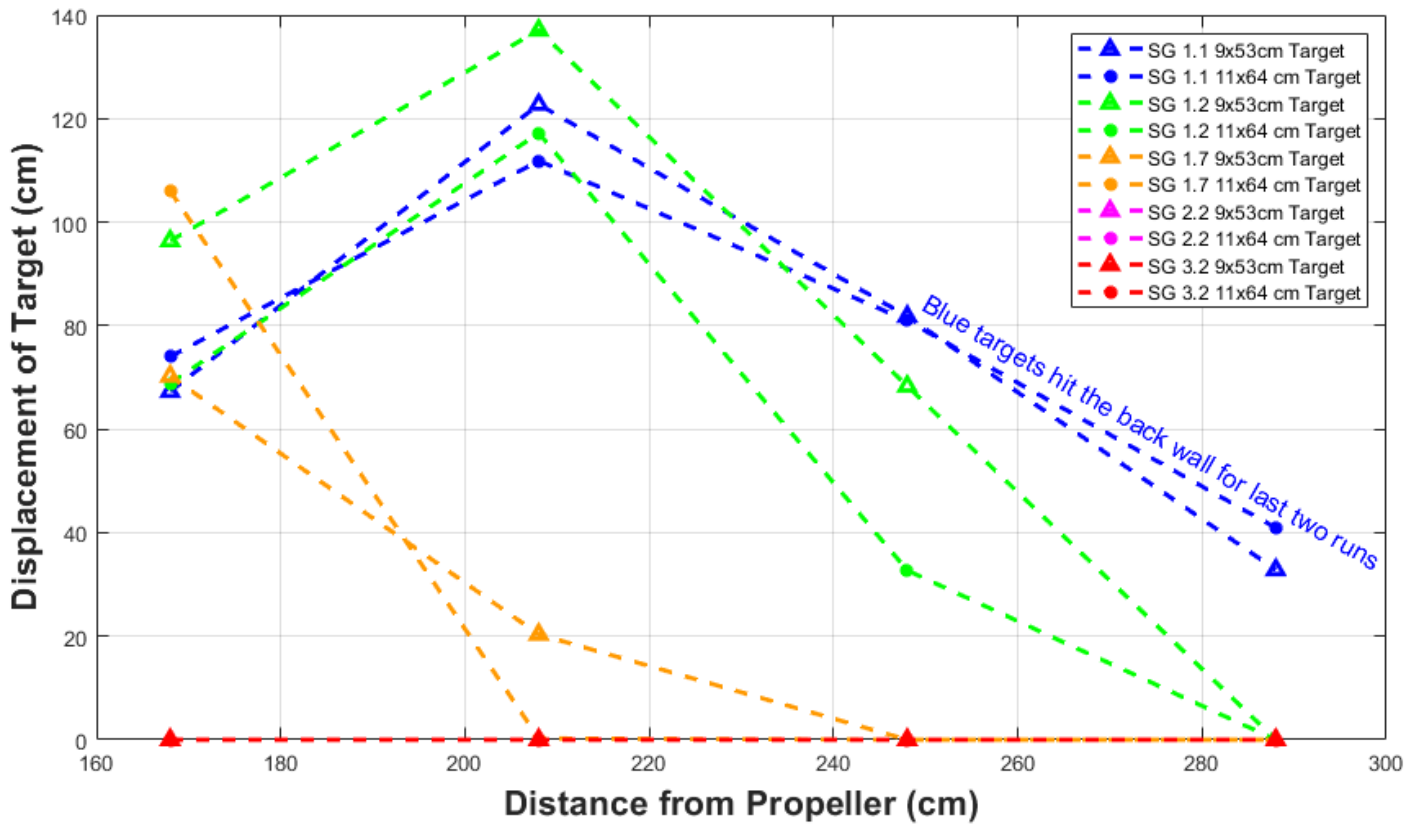


Figure 21. Target Displacement from Propeller Wash.

With the same propeller inputs as the rest of the targets, a test was also run on two M151070 Hydra Rockets with densities of 3.5 and 3.0 SG. The lighter 3.0 SG target spun by 15° but did not displace, while the 3.5 SG target did not move at all. The one-minute-long propeller test at the same RPM caused large displacement in the sediment bed in the shape of an elongated ellipse, deepest in the middle or center of the prop wash cone.

Using a GoPro for underwater video acquisition, the total suspended sediment mass displaced by the prop wash during the test runs was quantified at 33.6 kg. Quantification was achieved through a comparative analysis derived from a known reference trial. In the reference trial, the methodology established a relationship between the visible sediment displacement, and a measured 0.88 kg mass of sediment introduced in front of the camera. The reference and experimental footage were processed by converting each frame to grayscale intensity data. The quantification metric was the mean absolute change in pixel intensity within a defined Region of Interest (ROI), comparing frames under disturbance to a pre-disturbance baseline Reference Frame.

From Equation 02, the Reynolds Number was calculated for all targets (Table 09), and all tests had turbulent flow. As the targets SG and diameter increase, Re increases because the characteristic length and density increase with direct proportionality. The smallest and lightest target has a Re that is triple the value for Re to begin to transform from laminar flow to turbulent flow of 2300. The largest and heaviest target is 13x the transitional zone Re number.

Table 09. Reynolds number for each target.

1.1 SG	9 x 53 cm Target	14639
	11 x 64 cm Target	18821
1.2 SG	9 x 53 cm Target	15970
	11 x 64 cm Target	20532
1.7 SG	9 x 53 cm Target	22624
	11 x 64 cm Target	29088
2.2 SG	9 x 53 cm Target	29278
	11 x 64 cm Target	37643
3.2 SG	9 x 53 cm Target	42586
	11 x 64 cm Target	54754

The total Drag Force for each target depends only on the size as the drag coefficient, fluid velocity and fluid density are uniform throughout. The Drag Force for the 9 x 53 cm Target is 0.25 N and 0.37 N for the 11 x 64 cm Target. Similarly, the Lift Force only depends on size as well. The Lift Forces are 0.27 N and 0.40 N, respectively. The inherent buoyancy of the objects based off their displacement reduces the gravitational force affecting the normal and frictional forces as the targets rest in the sediment. All the targets have a SG greater than one and they sink. The buoyancy is 32 N for the 9 x 11 cm target, and the 11 x 64 cm target has 68 N.

Chapter 4

DISCUSSION

4.1 Optical Location for Maximum Displacement

For maximum displacement there is a starting position which correlates to the munition being placed where the prop wash field is strongest (Figure 23). The largest average displacement of 122 cm occurred for the 1.1 SG and 1.2 SGs when the propeller was located 208 cm away. Calculations (Hamil, 1999) indicate that the strongest forcing for this propeller and depth to sediment is located at 214 cm away from the hub closely matching the value found from the experiment.

4.2 Target Size and Density Differences

The smaller (9 x 53 cm) target moved farther than the larger target (11 x 64 cm) 75% of the time. The larger model has a larger surface area and experiences more hydrodynamic forcing for the same fluid velocity at the same density. However, the larger targets have more inertia, so they are more difficult to mobilize and have less time under the limited amount of propeller wash time to move. The smaller targets having less inertia require less momentum to maintain mobilization. The smaller targets accelerate faster in the prop wash and migrate farther once the initial peak thrust has passed. Recall the drag forces could not be scaled properly (Section 1.5), affecting the larger targets disproportionately. As expected, targets travelled less if they were far from the center of prop wash. The density was also inversely correlated with displacement.

4.3 Average Velocities

The average velocity of each target was estimated by taking the total displacement and dividing by the amount of time of prop wash (Table 10). It was assumed that the targets only moved while being acted upon by the propeller. Added to this known propeller time is added an extra 10% (0.5 s) for inertia, based on the underwater footage taken for each run.

Table 10. Average velocities for each test.

Distance to Propeller (cm)		168	208	248	288
1.1	9 x 53 cm Target	0.13	0.25	0.16	0.07
SG	11 x 64 cm Target	0.15	0.22	0.16	0.08
1.2	9 x 53 cm Target	0.19	0.27	0.14	0.00
SG	11 x 64 cm Target	0.14	0.23	0.07	0.00
1.7	9 x 53 cm Target	0.14	0.04	0.00	0.00
SG	11 x 64 cm Target	0.21	0.00	0.00	0.00
2.2	9 x 53 cm Target	0.00	0.00	0.00	0.00
SG	11 x 64 cm Target	0.00	0.00	0.00	0.00
3.2	9 x 53 cm Target	0.00	0.00	0.00	0.00
SG	11 x 64 cm Target	0.00	0.00	0.00	0.00

4.4 Shields Parameter

To find the Shields Parameter the bed stress was estimated. However, the rest of the equation is known (densities of the fluid, sediment, and mean particle diameter). The bed stress is estimated by:

$$\tau_{Bed} = \frac{1}{2} \rho_{fluid} U^2 C_f, \text{ where } C_f = \left(\frac{1}{4} \ln \left(\frac{30H}{2.5D_{50}} \right) \right)^{-2} \quad (06)$$

This equation calculates the friction coefficient based on sediment grain size (D_{50} is #30 Mesh) which comes out to 0.005, the total bed stress is 0.056 Pa. Plugging the bed stress into Equation 01, the Shields Parameter is 0.026. The critical Shields parameter is the specific value at which sediment particles first begin to move (incipient motion). With $\theta_{critical} = 0.033 - 0.045$ for turbulent flow, this suggests that the average bed shear stress is not quite strong enough to initiate wholesale transport of the median grain size. The local shear stress can be highly variable. Therefore, the above calculated $\theta = 0.026$ for this test suggests that the finest and least stable grains (those loosely packed or smaller than D_{50}) could be set in motion. All the suspended sediment that was witnessed are suggested to be the grains finer than D_{50} even though many fines were already washed out.

4.5 Froude Number

The Froude Number from Equation 03 is calculated to be:

$$Fr = \frac{0.15 \frac{m}{s}}{\sqrt{9.81 \frac{m}{s^2} \text{ Propeller Diameter (m)}}} \quad (07)$$

For the characteristic length of the propeller diameter (6" or 0.152 m), the Froude Number is 0.12. The Froude number characterizes the internal dynamics of the jet. It is a standard parameter used in modeling propeller-induced scour. Blaauw and van de Kaa (1975), and Hamill (1999) use the Froude number of the jet to correlate with the resulting scour depth or velocity decay rate. Using the propeller diameter as the characteristic length helps normalize the jet's behavior across different propeller sizes. Since $Fr \ll 1.0$ the flow is categorized as highly subcritical, indicating that the inertial forces of the jet are significantly overpowered by gravitational forces. The low Froude number is crucial because it confirms that the prop wash dynamics are uncoupled from free-surface effects (i.e., surface wave generation is negligible), allowing the study to focus purely on the flow interaction with the seabed. A low Froude number of 0.12 confirms that the flow

kinetic energy is focused almost entirely on generating turbulence and bed shear stress at the bottom boundary. Since surface wave generation is negligible, the calculated τ_{Bed} and subsequent Shields number θ are not being artificially reduced by energy dissipation into surface waves. Hence, why the Specific Gravity of the targets is the critical parameter in the findings. If gravity dominates the fluid, it follows that the primary force resisting the target movement is the submerged weight (a gravitational force).

4.6 Sliding Vs Rolling

When a force is applied to a cylinder, whether it rolls or slides depends primarily on the frictional interaction between the cylinder and the surface. Rolling occurs when static friction is sufficient to prevent the cylinder point of contact from slipping against the surface, creating a torque that causes rotation. Key parameters affecting this balance include the coefficient of static friction, the magnitude and direction of the applied force, and the cylinder mass and moment of inertia. When friction is high enough, the force produces a torque that initiates rolling. When friction is too low or the force too great, the cylinder slides with only kinetic friction opposing the motion but without rotation. In this case, the translational velocity V and angular velocity ω satisfy the no-slip condition of:

$$V = r\omega, \quad (08)$$

where r is the cylinder's radius. If the applied force exceeds the maximum static frictional force, slipping begins, and the cylinder slides instead of rolls.

Of the 18 targets that exhibited motion, 44.4% rolled, 33.3% slid. Motion type was unclear from the remaining 33% due to sediment suspension that prevented the video from capturing how they moved. As two targets exhibited both behavior and were counted for each, the total does not add up to 100%.

Table 11. Targets rolling vs sliding.

Distance to Propeller		168 cm	208 cm	248 cm	288 cm
1.1 SG	9 x 53 cm Target	Rolled	Rolled	Rolled	Unclear
	11 x 64 cm Target	Rolled	Unclear	Rolled then Slid	Rolled
1.2 SG	9 x 53 cm Target	Slid	Slid	Slid then Rolled	N/A
	11 x 64 cm Target	Slid	Rolled	Slid	N/A
1.7 SG	9 x 53 cm Target	Unclear	Unclear	N/A	N/A
	11 x 64 cm Target	Unclear	Unclear	N/A	N/A
2.2 SG	9 x 53 cm Target	N/A	N/A	N/A	N/A
	11 x 64 cm Target	N/A	N/A	N/A	N/A
3.2 SG	9 x 53 cm Target	N/A	N/A	N/A	N/A
	11 x 64 cm Target	N/A	N/A	N/A	N/A

Only the 1.2 SG targets showed an affinity for sliding (Table 11), while the 1.1 SG targets rolled more often. The 1.2 SG targets could have rolled at the end as the video footage only provides useful information for a brief time after the propeller is initiated as the disturbed sediment clouds vision. Decreasing hydrodynamic forces likely caused the targets to roll before reaching their final resting positions. The 1.7 SG targets had two factors working against them. First, having more inertia and being harder to move, they did not start moving as soon as the other targets. By the time they did start moving there was much more sediment suspended in the water column, and it was unclear to see if they did exhibit the behavior. Second, the sediment color while on land is a typical sand color, once saturated it takes on a darker hue to which the orange paint blended in well, making the targets hard to distinguish from the surrounding sediment.

Since mostly the 1.2 SG targets slid and using the average velocities from the nine cm target from Table 10 into Equation 09

$$\omega = \frac{v}{r} = \frac{(.19+.27+.14)\frac{m}{s}/3}{.0889 m / 2} = 13.5 \frac{rad}{s}. \quad (09)$$

It is most likely that all sliding cylinders began to roll once the applied prop wash force was less than the kinetic friction (which is less than the initial starting static friction), but this cannot be confirmed physically as the suspended sediment blocked visibility.

4.7 Some Targets Initially Moved the “Wrong Way”

7.5% of the targets initially showed a slight roll into the oncoming prop wash before being pushed in the direction of the prop wash as expected (Table 12). While it was only momentary (~ 0.5 s), it was visible and captured on the underwater footage.

Table 12. Targets that moved into prop wash initially.

Distance to Propeller		168 cm	208 cm	248 cm	288 cm
1.1 SG	9 x 53 cm Target	No	No	No	No
	11 x 64 cm Target	No	No	No	No
1.2 SG	9 x 53 cm Target	Yes	No	No	N/A
	11 x 64 cm Target	Yes	Yes	No	N/A
1.7 SG	9 x 53 cm Target	No	No	N/A	N/A
	11 x 64 cm Target	No	No	N/A	N/A
2.2 SG	9 x 53 cm Target	N/A	N/A	N/A	N/A
	11 x 64 cm Target	N/A	N/A	N/A	N/A
3.2 SG	9 x 53 cm Target	N/A	N/A	N/A	N/A
	11 x 64 cm Target	N/A	N/A	N/A	N/A

Only 1.2 SG targets that were experiencing the greatest thrust and moved the farthest exhibited this behavior. Note that two of these targets also slid, the 9 x 53 cm target at 168 cm from propeller and the 11 x 64 cm target at 208 cm from propeller. Two likely reasons for this action are scouring and vortices. The first method which is

disproven by the underwater footage would be scouring that appears on the front face of the target as the prop wash hits, is deflected down into the sediment, scours the sediment away creating a hole for the target to fall into.

The vortices are created as the fluid velocity increases when the propeller is brought up to speed and increases the Reynolds Number up from zero to its final turbulent value. From Equation 02, when the water is still ($v = 0$), $Re = 0$. As velocity increases, so does Re . For flow around a cylinder, once the flow separates, vortices appear behind the cylinder. In this situation and assuming minimal piping (flow under the target through the sediment), there is only one vortex behind the cylinder. Where the vortex contacts the cylinder, the vortex is pushing upwards and into the cylinder (Figure 25). The vortex could be the source of the movement.

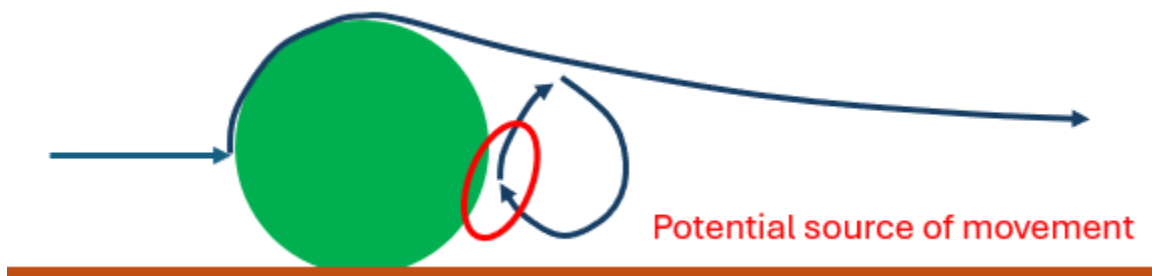


Figure 22. Potential non-symmetrical flow over a cylinder.

4.8 Lessons Learned

Many lessons were learned during this experiment and study. Some changes or alterations to the experimental plan would have been:

1) Conducting more tests with different parameters

Specifically, engine speeds (one slower and one faster), more SGs under 2.0 (1.3 and 1.45) and more target distances (148, 188, and 228 away from the propeller). Along the same train of thought would be to have the propeller farther away from the sediment box so the targets have more room to migrate so that no targets hit the back wall. While this would be a much larger testing matrix, it would only take one more month to complete. As some of the tests are already complete, and ~ half the tests can be skipped once realized which targets are not moving. Plus, at the end of the research, five tests were able to be completed each day in two hours once an efficient system was realized for all portions of the testing to include measuring, video set up, and most key, a non-pool diver to competently run the motor.

2) Repainting Orange Targets

The orange targets (SG 1.7) should be repainted to another color that is easier to see on video and do not blend into the sediment. The complimentary color of orange that contrasts deepest with the sediment is blue. As a deeper blue was already used, a lighter blue is recommended.

4) Less fine sediment particles

While small particulates are a naturally occurring phenomena, their presence in the laboratory settings greatly impedes visibility. A better method to filter out the fines would provide benefits during testing. Advantages to seek include a faster separating process as well as a process that pulls out more small diameter grains. Alternatively, one could source a better initial sediment sample and not deal with the problem at all.

5) Munitions with sensors inside

If the munitions had sensors inside them, this would be great advantage. First, if the set up was done properly, the initial and final locations could be found faster and more accurately. On top of this advantage, the instantaneous velocity and accelerations could be found. From this, the following characteristics could be calculated: inertia,

critical water velocity to initiate motion, momentum and momentum flux plus accurate rolling vs sliding for all targets no matter the turbidity.

6) Making sensor decisions more quickly

Finally, this is the largest take away for the author, making the decision more quickly to stop using equipment that is not producing expected results. Considerable time was dedicated to troubleshooting and resolving initialization issues with the Imagenex sonar unit. The effort, combined with the extended lead times for the required experimental components, resulted in a delay to the data acquisition phase of the project. After two months, working with manufacturers, other users, thorough review of the manual and troubleshooting with other researchers who have used instrumentation before it should have been abandoned. Instead, the team kept working with the sonar delaying completion of experimental tests.

Chapter 6

CONCLUSION

The thesis investigated the mobility of unexploded ordnance proxies subjected to propeller-generated turbulence in a controlled laboratory environment, focusing on the influence of specific gravity and propeller proximity. The primary objective was to define the critical hydrodynamic threshold required to initiate motion, addressing the risk of UXO migration by propeller wash.

The experimental results confirmed three major conclusions regarding the stability and mobilization of seabed munitions:

1. **Specific Gravity Dominance:** The target specific gravity (SG) was the most critical parameter governing mobility. Targets with $SG > 1.7$ demonstrated stability. A clear and consistent trend emerged indicating that targets with lower SG were more readily mobilized across a range of experimental conditions, a result that aligns with the predictions of Newton's Second Law of Motion. The finding underscores the fundamental relationship among mass, force, and acceleration, emphasizing that less dense objects require less force to initiate movement under otherwise equivalent loading scenarios.
2. **Propeller Proximity and Energy:** The experimental findings indicated a direct yet nonlinear relationship between the proximity of the propeller and target mobilization, emphasizing the critical role of jet energy distribution in driving target displacement. The experiments that observed the largest mobilization events were when the target was situated within the focal region of the propeller near-field jet, an area where maximal local flow velocities and elevated shear stresses

distinguish the region. Within this zone, the combination of concentrated turbulent momentum flux and high velocity gradients resulted in the greatest transfer of hydrodynamic energy to the sediment interface, echoing the spatially variable impact of jet-induced scouring described in propeller wash literature. Diminished shear stress produced lower magnitudes of displacement as the target location shifted away from the prop wash core.

In general, the population is safe from UXO as it is quite difficult to mobilize munitions on the seabed. The experiments demonstrated that initiating displacement of targets representative of conventional explosive ordnance (which typically possess high Specific Gravity) is extremely difficult. The findings suggest that historical dumping grounds located in deeper waters pose a lower mobility risk than previously assumed. The analysis limits the primary threat of propeller-induced mobility to scenarios where low density munitions are in active, shallow navigation channels or within confined port areas, such as Bravo Pier where munitions are loaded onto ships. However, the strategic location far away from other activities and the innate safety of ammunition movements means any lost UXO would immediately be run up the chain of command and dealt with by highly trained EOD divers.

References:

- Baranwal, A., Das, B. S. "Scouring around bridge pier: A comprehensive analysis of scour depth predictive equations for clear-water and live-bed scouring conditions." *AQUA*. 2024;73(2):424–452. doi:10.2166/aqua.2024.235
- Blaauw, H. G., van de Kaa, E. J. "Erosion of bottom and sloping banks caused by the screw race of maneuvering ships." Publ. no. 202. Delft, Netherlands: Delft Hydraulics Laboratory; 1978.
- Colangeli, C., Leftheriotis, G., Dimas, A., Brocchini, M. "Ship-Forced Sediment Transport: A New Model for Propeller Jet Flow." *Water*. 2024;16(12):1647. <https://doi.org/10.3390/w16121647>
- Cristaudo D, Gross BM, Puleo JA. Momentum balance analysis of spherical objects and long-term field observations of unexploded ordnance (UXO) in the swash zone. *J Mar Sci Eng*. 2023;11(1):79. doi:10.3390/jmse11010079
- Figlus, J., Kulesza, S., (2024) "Quantifying vessel propeller wash impacts on sedimentation in shallow-bay ports and waterways."
- Foster, D. S., Calantoni, J., Calvo, B. M., & Rennie, C. D. (2020). Initial motion of unexploded ordnance in the swash zone. *Continental Shelf Research*, 205, 104179.
- Ganju NK, Barnard PL, Hoover DJ, Xu X, O'Connell K. Storm and tidal interactions control sediment exchange in mixed-energy, mesotidal tidal inlet systems. *PNAS Nexus*. 2024;3(2):1-18.
- Hamill, G. A., Johnston, H. T., & Stewart, D. P. (1999). Propeller wash scour near quay walls. *Journal of Waterway, Port, Coastal, and Ocean Engineering*, 125(4), 170–175. [https://doi.org/10.1061/\(ASCE\)0733-950X\(1999\)125:4\(170\)](https://doi.org/10.1061/(ASCE)0733-950X(1999)125:4(170))
- Hamill, G. A., Johnston, H. T., & Stewart, D. P. (1999). Propel

- ler wash scour near quay walls. *Journal of Waterway, Port, Coastal, and Ocean Engineering*, 125(4), 170–175. [https://doi.org/10.1061/\(ASCE\)0733-950X\(1999\)125:4\(170\)](https://doi.org/10.1061/(ASCE)0733-950X(1999)125:4(170))
- Hong, J. H., Chiew, Y. M., & Cheng, N. S. (2013). Scour caused by a propeller jet. *Journal of Hydraulic Engineering*, 139(9), 1003–1012. [https://doi.org/10.1061/\(ASCE\)HY.1943-7900.0000746](https://doi.org/10.1061/(ASCE)HY.1943-7900.0000746)
- Idowu TE, Chapman E, Gangadharan MK, Stolle J, Puleo JA. Nearshore migration of munitions and canonical objects under large-scale laboratory forcing. *J Mar Sci Eng*. 2024;12(11):2103. doi:10.3390/jmse12112103
- Landa, J. T., Foster, D. S., & Calantoni, J. (2020). *Analysis of Unexploded Ordnance Mobility at the Formerly Used Defense Site, Culebra, Puerto Rico*. U.S. Army Corps of Engineers, Engineer Research and Development Center.
- Lam, W. H., Hamill, G. A., Song, Y. C., Robinson, D. J., & Raghunathan, S. (2011). A review of the equations used to predict the velocity distribution within a ship's propeller jet. *Ocean Engineering*, 38(1), 1–10. <https://doi.org/10.1016/j.oceaneng.2010.10.016>
- Leishman JG. *Introduction to Aerospace Flight Vehicles*. Published by the author; Copyright 2022–2025.
- Mujal-Colilles, A., Castells, M., Llull, T., Gironella, X., & Martínez de Osés, X. (2018). *Stern twin-propeller effects on harbor infrastructures. Experimental analysis*. *Water*, 10(11), 1571. <https://doi.org/10.3390/w10111571>
- Ong, D. M., Merkouris, P., & Fitzmaurice, M. (Eds.). (2010). *Research Handbook on International Environmental Law*. Cheltenham, UK; Northampton, MA: Edward Elgar Publishing.
- Oldenhof, M. (2021). *Understanding the development and behavior of scour holes in rivers: Hydrodynamic and geotechnical conditions*. University of Twente. https://research.utwente.nl/files/447501916/MartheOldenhof_LiteratureStudy_ScourHoles_.pdf
- Salim, S., Pattiaratchi, C., Tinoco, R., et al., (2018). Sediment Resuspension Due to Near-Bed Turbulent Effects: A Deep Sea Case Study on the Northwest Continental Slope of Western Australia. *Journal of Geophysical Research: Oceans*, 123(10), 7102-7119.
- SERDP, (2018) “Final Report”, Workshop on Acoustic Detection and Classification of Munitions in the Underwater Environment, Reston, VA.
- SERDP, (2010) “Munitions in the underwater environment: state of the science and knowledge gaps”, Report, SERDP/ESTCP.
- Shields A. Application of similarity principles and turbulence research to bed-load movement (translated version). *Mitteilungen der Preußischen Versuchsanstalt für Wasserbau*. 1936;26. Berlin: Preußische Versuchsanstalt für Wasserbau.
- Stauber, Rick. "History of Munitions Dumping." Presented at: Federal Region III Regional Response Team Conference; May 23, 2018; Philadelphia, PA.

- Sumer BM, Fredsøe J. *Hydrodynamics Around Cylindrical Structures*. Revised ed. World Scientific Publishing; 2006. doi:10.1142/6248.
- Tan, R. İ., Yüksel, Y., & Çelikoğlu, Y. (2016, November 17–20). Propeller jet flow, pile supported piers and sea bed interaction. In *35th International Conference on Coastal Engineering (ICCE)* (pp. 1–8). Antalya, Türkiye: Coastal Engineering Proceedings.
- Trembanis AC, DuVal C. Unexploded Ordnance Characterization and Detection in Muddy Estuarine Environments. SERDP Project MR-2730. University of Delaware; 2017.
- Whitehouse, R. J. S., R. L. Soulsby, W. G. M. Davies, and P. S. F. Tappin. (2011). *Scour at Marine Structures: Processes and Prevention*. CRC Press, Taylor & Francis Group.
- Zanke, U. C. E. (2003). On the influence of turbulence on the initiation of sediment motion. *International Journal of Sediment Research*, 18(1), 17–31. [https://doi.org/10.1016/S1001-6279\(03\)70002-5](https://doi.org/10.1016/S1001-6279(03)70002-5)